Identification of Lithium Hydride and its Hydrolysis Products with Neutron Imaging

E. Garlea[a], M. O. King[b,*], E. C. Galloway[b], T. L. Boyd[a], N. R. Smyrl[a], H. Z. Bilheux[c], L. J. Santodonato[c], J. S. Morrell[a], J. H. Leckey[a]

[a] *Y-12 National Security Complex, P.O. Box 2009, Oak Ridge, TN 37831, USA*
[b] *AWE plc, Aldermaston, Berkshire, RG7 4PR, UK*
[c] *Oak Ridge National Laboratory, Oak Ridge, TN 37831, USA*

Abstract

In this study, lithium hydride (LiH) and its hydrolysis products were investigated non-destructively with neutron radiography and neutron computed tomography. Relative neutron transmission intensities (I/I_0) were measured for LiOH, Li_2O and LiH, and their linear attenuation coefficients calculated from this data. We show that ^{7}Li is necessary for creating large differences in I/I_0 for facile identification of these compounds. The thermal decomposition of LiOH to Li_2O was also observed with neutron radiography. Computed tomography shows that the samples were fairly homogeneous, with very few macroscopic defects. The results shown here demonstrate the feasibility of observing LiH hydrolysis with neutron imaging techniques in real time.

1. Introduction

Lithium hydride (LiH) is a light, hydrogen dense material which has received attention due to its use as a hydrogen storage medium [1–7], whilst its corrosion products, particularly Li_2O, has been studied as candidate tritium breeding materials for use in commercial nuclear fusion [8–10] and as a electrode material in Li-ion batteries [11]. LiH reacts readily with moisture to irreversibly form surface corrosion layers of Li_2O, LiOH and $LiOH \cdot H_2O$ [12–19]. This poses problems for storage and handling and the material must be kept and processed in vacuum or an ultra-dry inert gas glove box. Even in these conditions, the material slowly hydrolyzes due to trace quantities (less than 1 ppm) of moisture [20, 21]. Corrosion layer thickness varies in size and morphology with the environmental conditions [22–24]. On the other hand, controlled LiH hydrolysis has been proposed as an efficient hydrogen generator for portable applications [3, 5, 6]. Hydrolysis is given by either:

$$2\,LiH + H_2O \longrightarrow Li_2O + 2\,H_2 \tag{1}$$

$$Li_2O + H_2O \longrightarrow 2\,LiOH \tag{2}$$

Alternatively:

$$LiH + H_2O \longrightarrow LiOH + H_2 \tag{3}$$

$$LiH + LiOH \longrightarrow Li_2O + H_2 \tag{4}$$

In both these reaction schemes, a thin layer of Li_2O forms at the interface between LiH and LiOH. This process is thought to be a diffusion limited process and results in a trilayer LiH – Li_2O – LiOH corrosion system. There is a growing consensus, both experimentally and theoretically, that under ambient conditions, the hydrolysis reaction proceeds via the formation of Li_2O before LiOH (*i.e.* formed by equations 1 and 2) [12, 16, 25, 26]. In other words, Li_2O is favored by lower moisture exposures and at higher temperatures. At 298 K, the thickness of the Li_2O layer is reported to be in the 10 nm range [16]. Upon heating to 523 K, the conversion of LiOH to Li_2O has been observed on a LiH substrate [14, 22, 27]:

$$2\,LiOH \longrightarrow Li_2O + H_2O \tag{5}$$

Several analytical techniques have been applied to study these reactions, including infrared spectroscopic methods, x-ray diffraction, gas pressure measurements or thermal decomposition methods. By measuring the –OH resonance, diffuse reflectance infrared Fourier transform (DRIFT) spectroscopy has shown the presence of LiOH on the surface of LiH following exposure to moisture. DRIFT spectroscopy has also shown that –OH is lost upon heating, with hydroxide being converted to oxide [14, 21, 28]. Raman spectroscopy has also been recently applied to the study of LiH corrosion, in particular the measurement of the Li_2O phonon [29–31]. Thermal decomposition and diffraction have provided kinetic and mechanistic information on the hydrolysis of LiH [20] and the subsequent thermal decomposition of the LiOH layer [22–24].

Neutron characterization offers an alternative and as yet unexplored method of probing the nature of LiH and its hydrolysis products. Antecedent studies of LiH with neutrons have, for example, focussed on crystallography

*Corresponding author
Email address: martin.king@awe.co.uk (M. O. King)

[32] and Compton scattering experiments [33]. The use of LiH as a neutron shielding material has also recently been discussed [34]. As opposed to x-ray radiation, neutrons interact strongly with Li and H and thus are attractive as a probe of LiH and its corrosion products. X-ray attenuation is related to the atomic number of the atoms present in a material and therefore LiH is amongst the poorest x-ray absorbers. In the case of neutrons, attenuation is determined by the nuclear structure of a particular atom, with natural Li and H exhibiting very high attenuation characteristics. In this report, neutron radiography and computed tomography (CT) data are obtained for the LiH corrosion system. The main goal of these measurements were to experimentally determine the relative transparencies of LiH, Li_2O and LiOH to cold neutron irradiation. We also wished to observe the thermal dehydration of LiOH with neutron techniques and therefore to evaluate the possibility of imaging LiH corrosion in real time.

2. Experimental

2.1. Materials

Samples were produced from the compaction of powders at ∼20.7 MPa (3000 psi) in a uniaxial Carver die press using a 6 mm diameter die set. Micron sized LiOH and Li_2O powders were first pressed in laboratory atmosphere, which took approximately 10 minutes, otherwise they were stored in a dry Ar glove box. The laboratory was maintained at 293 K and had a relative humidity of about 45%. The LiOH/Li_2O sample and the die set were placed in the glovebox, where the LiD powder was loaded. The whole sample was sealed in a polyethylene bag, removed from the glovebox and pressed. At no point was the containment of the polyethylene bag broken, hence the LiD layer was not exposed to laboratory atmosphere. To ensure sufficient neutron transmission, each 6 mm sample was sanded down in the glovebox, by hand, to a thickness of 3 mm parallel to the neutron transmission axis.

Table 1 shows the isotopic composition of the samples used here. The reason for selecting Li compounds enriched with ^{7}Li is two fold. Firstly, samples containing natural Li have sufficient ^{6}Li to prevent any neutron transmission being observable. Secondly, we wish to observe LiH chemistry and thus we are interested in spatial distributions of H and O and therefore variations in attenuation due to Li is not of particular interest; O and H are the mobile species in this system. Instead of using LiH enriched with the ^{7}Li isotope, the decision was made to use Li^{2}H which reduces neutron attenuation via the use of the ^{2}H (D) isotope. We note that the use of ^{7}Li [35] and D [36] in neutron characterization experiments has previously been described. Also the use of D afforded the possibility of observing D mobility in the Li_2O and LiOH layers after thermal treatment. As shown in table 1, the LiH samples are predominantly ^{2}H and will be referred to henceforth as LiD. Also for brevity 99.99% ^{7}LiOH will be refered to as LiOH. LiD samples were approximately 90% dense compared to the theoretical maximum calculated from x-ray diffraction [16, 37]. Li_2O and LiOH both exhibited densities in the region of 95–98% of their theoretical densities [16].

Table 1: Isotopic composition of the samples used in this study. Note that Li_2O (2) was produced via heat treatment of LiOH, see table 2 for details. Natural O was used in all samples.

Compound	Isotopic Composition (%)			
	^{6}Li	^{7}Li	^{1}H	^{2}H
LiH	7.59	92.41	8	92
LiOH	0.01	99.99	99.99	0.01
Li_2O (1)	2	98		
Li_2O (2)	0.01	99.99		

Five samples were produced, four layered and one a mixture of powders. A summary of sample composition, nominal layer thickness and thermal treatment is presented in table 2. Of the four layered samples, the thickness of the Li_2O layer was varied (0.05 mm and 0.16 mm) to assess its effect on reducing further hydrolysis of the LiD during the thermal decomposition of LiOH (equation 5). This effect is known to occur in samples containing native corrosion products of LiD, in that further hydrolysis is a diffusion limited process across the Li_2O layer [22, 24]. We note that these Li_2O layers are too large to be considered representative of the ambient LiD hydrolysis system but they still have the ability to give useful H_2O transport information across the Li_2O layer. Thermal treatment was performed *ex-situ* on samples 1 and 5. Samples were removed from the glovebox, wrapped in Al foil before being transported briefly in air to be loaded in an Al vessel. The Al vessel was immediately evacuated to a pressure of approximately 3 Pa. The vessel was placed in a tube furnace and was heated in 100 K increments to a final temperature of 673 K in about 30 minutes. The temperature was monitored using a K-type thermocouple positioned on the vessel. Pressure increased to 7.4 Pa immediately after the temperature of 673 K was reached and returned to 3 Pa after 45 minutes at temperature. After 3 hours, the furnace was turned off and samples were left in the tube to cool, while maintaining the vacuum.

2.2. Neutron Imaging

Neutron radiography was performed using the CG-1D imaging instrument at the High Flux Isotope Reactor, situated within Oak Ridge National Laboratory (ORNL) (Tennessee, USA) [38]. The instrument provides a cold polychromatic neutron beam with a wavelength spread of 0.08 – 0.6 nm, with an intensity maximum at 0.26 nm. The overall neutron flux is estimated to be 5×10^6 cm^{2}s^{-1}. Neutron radiographs were captured on a LiF/ZnS scintillator attached to a charge coupled device (CCD) camera

Table 2: Chemical composition and thermal treatment of samples used in this study. The dimensions given are nominal. The pressure refers to the base pressure during heat treatment. Thermal treatment of LiOH converted it to Li_2O (2).

Sample	Layer thickness (mm) LiD : Li_2O (1) : LiOH	Thermal Treatment
1	1 : 0.05 : 1	673 K, 3 h, 3 Pa
2	1 : 1 : 1	
3	powder LiD / LiOH	
4	1 : 0.16 : 1	
5	1 : 0.16 : 1	673 K, 3 h, 3 Pa

which has a field of view of $28 \times 28\,\mathrm{mm}^2$. The camera was Peltier cooled to about 210 K to reduce thermal noise in the electronics. The resolution of the instrument was determined with a Gd coated grid to be approximately 100 µm. To collect CT data, each sample was rotated through 180° at an increment of 0.17°.

Neutron imaging relies on the attenuation of a neutron beam as it traverses a given material. For each pixel (x, y) the observed neutron flux, I, as a beam of neutrons transverse a sample is given by the *Beer-Lambert law* [39–41]:

$$I(x, y) = I_0(x, y) \exp(-\Sigma(x, y) d(x, y)) \tag{6}$$

where I_0 is the incident neutron flux, Σ is the linear neutron attenuation coefficient and d is the sample thickness, in the direction parallel to the neutron beam.

At each angle a two dimensional radiograph was obtained with an acquisition time of 85 s. Prior to imaging the samples, a dark field and an open beam image were recorded. The dark field image was obtained with the neutron beam stopped to record any dark currents in the CCD apparatus. The open beam image was collected for a neutron beam without any sample, which is equivalent to the incident beam intensity, I_0. With a sample placed in the beam, the intensity on the detector was then the uncorrected transmitted beam intensity, I'. Since the samples were enclosed within an Al vessel (to prevent atmospheric corrosion), the effect of the neutron attenuation from the sample holder must be accounted for. The corrected relative transmission (I/I_0) of the sample is therefore:

$$\frac{I}{I_0} = \frac{I'}{I_0} + \frac{I_a}{I_0} = \frac{I' + I_a}{I_0} \tag{7}$$

where I' is the uncorrected transmission and I_a is the attenuation due to the Al can. The relative transmission of the Al can was measured to be 0.93 in a region close to the samples, hence the relative attenuation (I_a/I_0) is 0.07. This value is added to each measurement of I'/I_0 to give I/I_0. In all figures and tables, the corrected relative transmission is given.

2.3. Chemical Characterization and Microscopy

In addition to neutron imaging, the pressed samples were studied with optical microscopy and Raman spectroscopy. Specifically, similar samples were evaluated by optical microscopy in air, before and after the heat treatment to evaluate if dimensional changes with temperature and pressure occurred. Raman spectroscopy was conducted on the Li_2O sample to confirm its integrity and also on a heat treated sample at different locations. Each sample was contained in a CF40 cell with a glass window for Raman data acquisition. The instrument utilized was a B&W TEK i-Raman Plus with a microscope attachment (20x objective) with 532 nm excitation.

3. Results and Discussion

3.1. Preliminary Characterization

Optical images of a LiD / Li_2O (1) / LiOH sample is shown in figure 1. It shows a sample of nominal dimensions of 1 mm : 0.16 mm : 1 mm, pre and post heating (equivalent to samples 4 and 5, respectively, in table 2). The layer thickness was measured to be LiD – 1255 µm, Li_2O – 118 µm, and LiOH – 1000 µm. The observed roughness of these layers is $\sim$ 50 µm and $\sim$ 10 µm for the LiD – Li_2O (1) interface and the Li_2O (1) – LiOH interface, respectively. After heat treatment, it was observed that LiD was covered with a white coating, especially at the edges of the layer and there was also evidence of separation of LiOH from Li_2O. Within the limits of the interface roughness, there was no measurable change in layer thickness after the heat treatment. The white coating on this sample was identified by Raman to be LiD with a minor amount of Li_2O, figure 2(a). This Raman spectrum shows a broad feature centered around 2600 cm^{-1} which is likely to be LiD fluorescence similar to that previously observed for LiH [30]. The symmetric stretch for Li – O – Li is barely discernible at 517 cm^{-1}. There was spatial variation in the intensity of the Li_2O feature, indicating that there was a dispersion of Li_2O within the LiD matrix. Also characterized by Raman was the Li_2O layer. This was done to check for Li_2O hydrolysis when the sample was briefly exposed to atmosphere for pressing and thermal treatment. Figure 2(b) show a typical Raman spectrum for this layer, revealing that it was predominantly Li_2O with minor amounts of LiOH (at 3666 cm^{-1}) and Li_2CO_3 (at 1594 cm^{-1} and 1089 cm^{-1}) [14]. We conclude by stating that both LiD and Li_2O layers are of high purity with only a minor amount of other compounds detectable.

3.2. Neutron Radiography

3.2.1. Neutron Radiography – Imaging

Representative neutron radiographs of LiD and its related corrosion products are shown in figure 3. The composition of samples in figure 3 are annotated on the figure and described in more detail in table 2. They show strong contrast between the LiD, LiOH and Li_2O (2) (99.99%

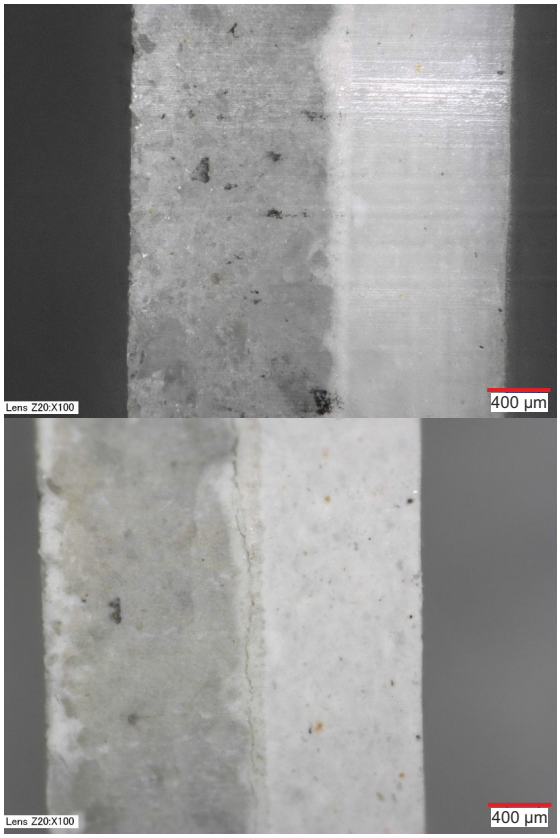

Figure 1: Optical microscopy of LiD / Li_2O (1) / LiOH sample prior to and after thermal treatment (673 K) in rough vacuum (3 Pa). The left hand layer is LiD, the middle layer is Li_2O (1) and the right hand layer is LiOH.

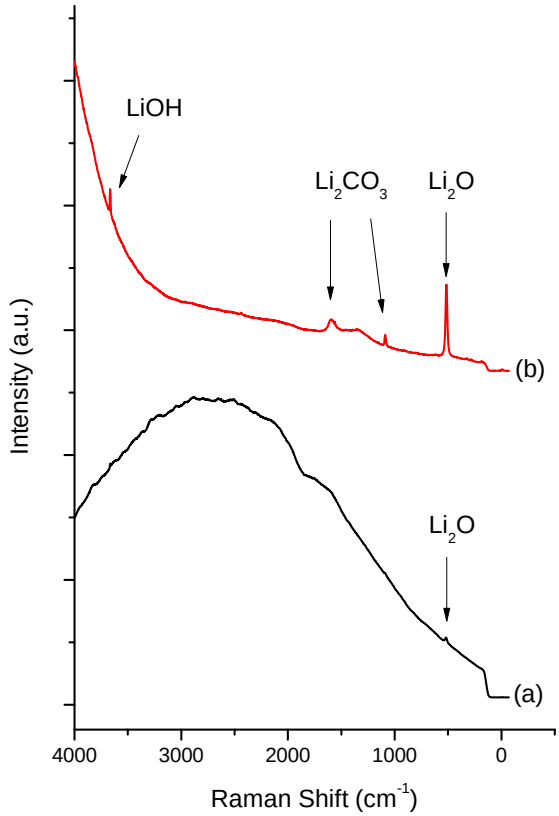

Figure 2: Raman spectra of (a) LiD portion of thermally treated LiD / Li_2O (1) / LiOH sample, showing a minor Li_2O feature; (b) as fabricated Li_2O sample, containing minor amounts of LiOH and Li_2CO_3.

^{7}Li) layers of each sample. The LiD layer in each sample is rather opaque to neutrons, while the Li_2O (2) layer is highly transparent to neutrons. The Li_2O (1) (98% ^{7}Li) and LiOH layers are both relatively strong neutron absorbers due to their ^{6}Li and H content, respectively. Samples (2) and (4) particularly show that there is very little difference in relative transmission between the Li_2O (1) and the LiOH layers. The intention of sample (3), a mixture of LiD and LiOH, was to observe the solid state reaction between LiD and LiOH (equation 4). It is clear that there is an increase in neutron transparency compared to pure LiD, which is a result of the presence of the less attenuating LiOH. The generation of Li_2O would reduce neutron attenuation further and thus may cause localized variations in neutron transparency. Although there is evidence that there are variations in neutron transparency, it is difficult to say whether these are a result of variations in O distribution due to Li_2O or LiOH; or are simply an artefact of the mixing process. Layered samples provide much more certainty in the assignment of compounds and the chemistry involved. Samples (1), (4) and (5) were prepared to explore the thermal decomposition of LiOH (equation 5) and the effect of the evolved H_2O on LiD, albeit with a artificially thicker Li_2O (1) layer than occurs naturally. Comparing samples (4) and (5), it is clear that the LiOH layer has decomposed to Li_2O. The only plausible explanation is that the strongly attenuating H has been lost from this material, as per equation 5. To ascertain the effect of LiOH decomposition on LiD, it was necessary to examine line profiles of the neutron radiographs, which are described in the next section.

3.2.2. Neutron Radiography – Line Profile Analysis

We now turn to the main purpose of this study: the quantification of neutron radiographs. To do this, line profiles were obtained across the layers, which are displayed in figure 4. Line profiles are displayed for samples (1), (2) and (5). A line profile for sample (3) does not make sense and sample (4) has essentially the same profile as sample (2) albeit with a smaller Li_2O (1) layer, hence these profiles are not displayed. The large differences in neutron transparency, among LiD, Li_2O (2) and LiOH represents a chemical fingerprint to easily identify the compound involved in the hydrolysis of LiH. This effect could be exploited in future studies to view hydrolysis in real time or to map the extent of the hydrolysis reaction in three dimensional space, similar to what has been demonstrated for H_2O transport in concrete [42], soil [43] and fuel cells [44]. The red line in figure 4 shows that the difference

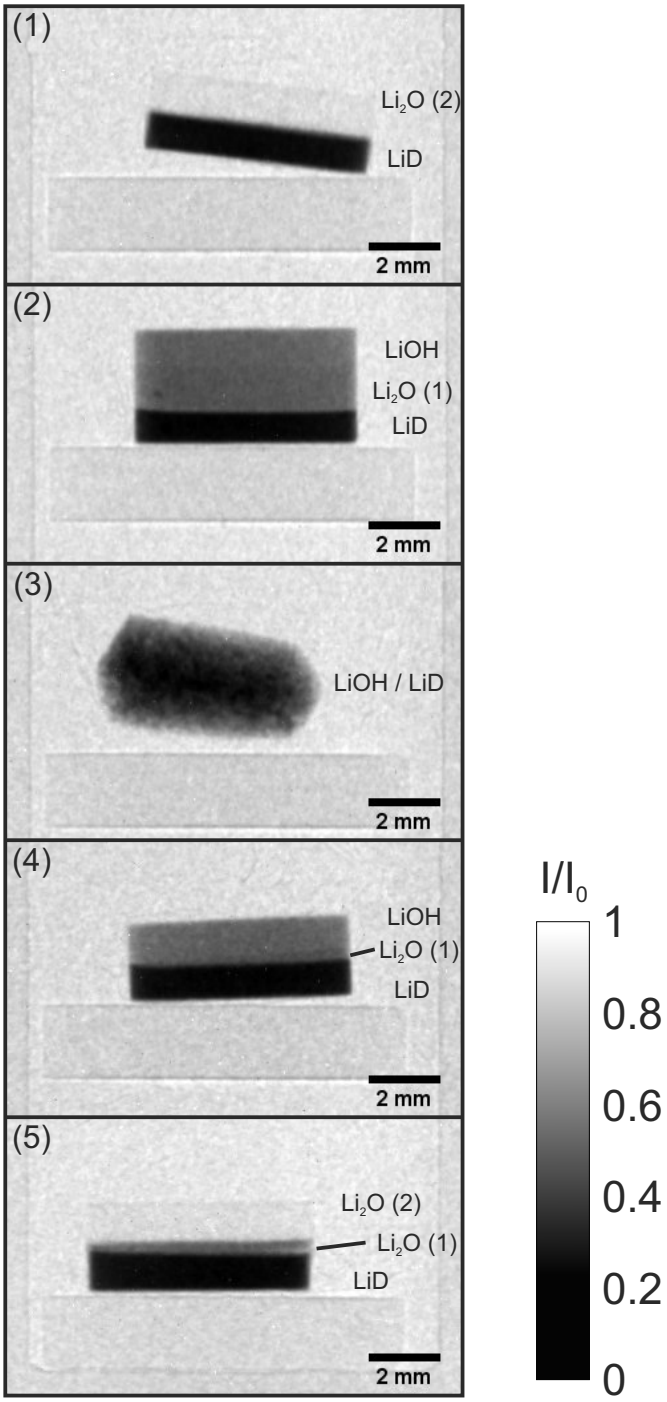

Figure 3: Representative neutron transmission radiographs obtained for samples 1 to 5 (see table 2 for details). The isotopic composition of Li_2O (2) and LiOH is 99.99% ^{7}Li while Li_2O (1) has 98% ^{7}Li. LiD is natural Li.

in neutron transparency between Li_2O (1) and LiOH is rather slight, the two layers are only just discernible from each other, with the difference being about 4%. A direct comparison can be made of the neutron absorption between Li_2O (1) and Li_2O (2). A 3 mm sample of Li_2O (1) attenuates 49% of neutrons while Li_2O (2) attenuates just 4% of neutrons.

The line profiles also provide information on surface roughness and thus may indicate reactions occurring at material interfaces. Sample (2)'s line profile indicates that the interface is ∼200 µm wide. This is slightly broader than the interfacial roughness measured by optical microscopy, probably due to the fact that neutron radiography penetrates the whole sample while optical microscopy is essentially a surface measurement. This sample has had no thermal treatment and thus the roughness measured from this sample is the natural roughness of the interface.

The line profile of sample (1) (blue line in figure 4) shows that the interface is broader than sample (2), ∼450 µm. Sample (1) contains a Li_2O (1) layer that is nominally 50 µm thick. This leaves a difference of about 200 µm, which is either: an increase in roughness due to a degree of delamination as in sample (5); or thermally induced hydrolysis of the LiD layer, through liberation of H_2O from the LiOH layer. Optical microscopy (figure 1) would suggest that thermally induced delamination of this sample is rather small (of the order of 10 µm), while the whitening (Li_2O formation) at the interface is of the order of 100 µm, which is consistent with the neutron imaging. As LiD is formed of natural LiH, hydrolysis of this layer would mean that the neutron transparency of this layer would tend toward Li_2O (1) with a relative transmission of 0.51, consistent with line profile analysis.

In addition, the LiD – free space interface was measured. It has a similar roughness (∼220 µm) before and after thermal processing, according to neutron radiography. Optical microscopy, figure 1, suggests that oxide layer at the outside of the LiD layer is ∼150 µm thick. The lack of any difference in the neutron radiography (a bulk measurement) between pre and post thermal treated samples would suggest that hydrolysis at this interface is a surface effect and does not penetrate particularly far into the bulk of the material. Raman spectroscopy (figure 2) is supportive of this assertion as the data shows that Li_2O is only present in small quantities on the LiD surface.

The linear attenuation coefficient, Σ, can be measured from experiment, as described by equation 6. It can also be estimated from the physical properties of the material. Σ is given by [45]:

$$\Sigma = \sigma(\lambda)N = \sigma(\lambda)\frac{\rho N_A}{M} \tag{8}$$

where Σ is the linear attenuation coefficient, $\sigma(\lambda)$ is the total neutron cross section for neutrons of wavelength λ, N is the atom density, ρ is the material density, N_A is Avogadro's number and M is the molar mass. The total neutron cross section is the sum of the scattering and ab-

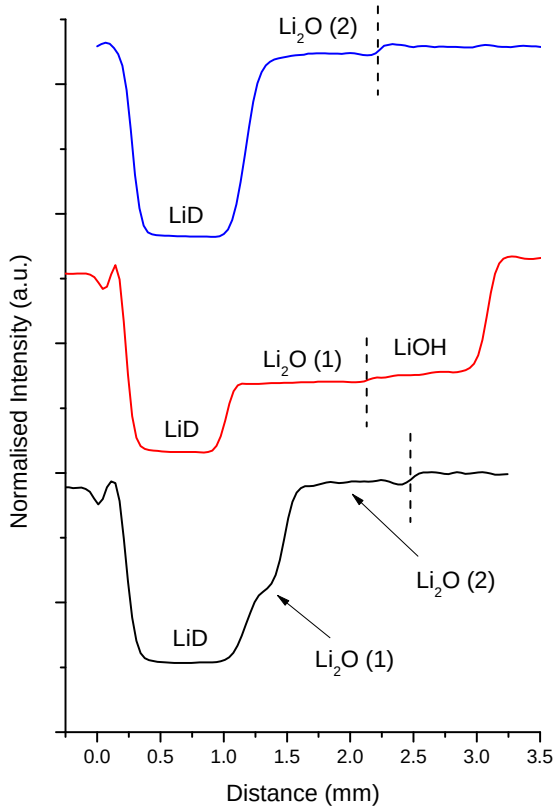

Figure 4: Line profiles derived from figure 3. Blue line: line profile from sample (1), Li_2O (2) / Li_2O (1) / LiD. Red line: sample (2) LiD / Li_2O (1) / LiOH. Black line: sample (5) and LiD / Li_2O (1) / Li_2O (2). Li_2O (2) and LiOH have 99.99% ^{7}Li content while Li_2O (1) has 98% ^{7}Li.

sorption cross sections. Table 3 shows the absorption and scattering cross sections for isotopes relevant to this study. Table 4 shows the physical properties; derived and measured values of Σ; and the expected and measured I/I_0 for a 3 mm thick sample.

Table 3: Thermal neutron (λ= 0.18 nm) cross section data for relevant elements and isotopes. σ_s is the neutron scattering cross section and σ_a is the neutron absorption cross section. Data sourced from [40, 46–49].

Element	σ_s (barns)	σ_a (barns)
^{1}H	82.02	0.33
^{2}H (D)	7.64	5×10^{-4}
^{6}Li	0.97	940
LiH	1.37	70.5
98% ^{7}Li	1.39	18.85
^{7}Li	1.40	0.05
O	4.23	2×10^{-4}

As can be seen in table 4, deviations between calculation and experiment exist. The reasons for which will now be discussed. Applicable to all materials is the fact we have used a cold neutron source (λ= 0.08 – 0.6 nm, peaked at 0.26 nm), but the calculations are performed with thermal neutrons (λ= 0.18 nm). This will cause greater attenuation due to the fact that neutrons have a higher cross-sections in the cold range. However, as can be seen in table 4, attenuation in some materials is actually lower, hence the cold source cannot be the only reason why deviations occur.

In terms of particular materials, the values obtained for I/I_0 and Σ for LiD and Li_2O (2) are in reasonable agreement with the calculated values. Transmission is slightly higher in both cases. Much of the deviation can be accounted for by noting that the density of these materials is less than the theoretical maximum. In the samples used here, LiD was measured to be ∼90% dense, while Li_2O (1) and LiOH were measured to be 95–98% dense. If one applies a correctional factor of 0.9 and 0.95 to the calculated values of I/I_0 for LiD and Li_2O (2), respectively, then it improves the agreement between calculated and measured values. Furthermore, the Li_2O (2) layers have been formed by the dehydration of LiOH. Escape of H_2O during this process has been shown to cause spallation and cracking and thus will increase the porosity of the material [22–24], further increasing neutron transmission. For Li_2O (1), the measured I/I_0 is lower (more attenuating) than expected from calculation. This is likely a result of contamination. The Li_2O (1) layer was formed in ambient laboratory conditions, which has been shown in figure 2 to contain small but detectable levels of LiOH and Li_2CO_3. LiOH contains H, hence it is a more effective neutron moderator and may explain why the observed attenuation is slightly greater than the calculated value.

On the other hand, there are significant differences between the value obtained for Σ from calculation and ex-

Table 4: Relative neutron transmission (I/I_0) of compounds relevant to this study. ρ is material density, M is molar mass, N is the atom density, Σ is the linear attenuation coefficient, which was calculated from equation 8. Percentages refer to the isotopic concentration of ^{7}Li, except LiD where it is labelled individually. The calculated values of Σ assume idealize material composition and no beam hardening effects.

Compound	ρ	M	N	Σ (cm^{-1})		I/I_0	
	(g cm^{-3})	(g mol^{-1})	($\times$ 10^{22} cm^{-3})	Calc.	Exp. ($\pm$ 0.15)	Calc.	Exp. ($\pm$ 0.01)
92% LiD 8% LiH	0.86	8.86	5.86	5.00	4.36	0.22	0.27
99.99%^{7}LiOH	1.47	23.98	3.65	3.21	1.99	0.38	0.55
98% ^{7}Li$_2$O (1)	2.02	29.98	4.05	1.81	2.24	0.58	0.51
99.99% ^{7}Li$_2$O (2)	2.02	29.99	4.05	0.29	0.13	0.92	0.96

periment for LiOH. The experimentally obtained attenuation parameters for LiOH is significantly less attenuating than would be expected from calculation. Beam hardening, whereby low energy neutrons are preferentially removed, may contribute to the observed deviations in I/I_0 and Σ for this material. Several mathematical models have been produced to correct for beam hardening [50–52], however, the application of them here lies outside the scope of this study. This effect will shift the observed I/I_0 to a higher value and will therefore reduce the observed Σ. It is known to be particularly evident in strong neutron absorbers, hence it would be expected to contribute here.

3.2.3. Neutron Radiography – Tomography

CT allowed for the three dimensional visualization of the LiD, Li$_2$O (1), Li$_2$O (2) and LiOH layers. A three dimensional rendered volume of samples (4), (2) and (1) are shown in figures 5(a), (b) and (c), respectively. In sample (4), the LiD layer is clearly discernible from the LiOH layers; however, the Li$_2$O (1) / LiOH interface is indistinct with a boundary that is not easily identifiable. There is a small defect evident at the surface of LiD layer. The sample appears to have been chipped which probably occurred during sample fabrication.

Figure 5(b) shows a three dimensional rendered volume of sample (2). The main difference between this and figure 5(a) is that the Li$_2$O (1) layer is larger. Again the boundary between the Li$_2$O (1) and LiOH layers is unclear. It also reveals that this sample is highly homogeneous within each layer, with only a small defect visible at the LiD / Li$_2$O (1) interface, which was possibly introduced into the sample during pressing. Line profile analysis, figure 4, is the more reliable method for distinguishing between these two layers. In addition, the tomography of this sample reveals highly neutron attenuating impurities, which appear as two near spherical intense red features in figure 5(b). These impurities are likely to be a result of contamination during sample preparation.

Figure 5(c) shows a two dimensional cut through sample (1). The Li$_2$O (2) layer was too transparent to be effectively depicted as a colormap, hence a grayscale image is presented here. The two dimensional cut through the LiD / Li$_2$O (2) sample revealed only a small amount of roughness observable at the interface. During thermal

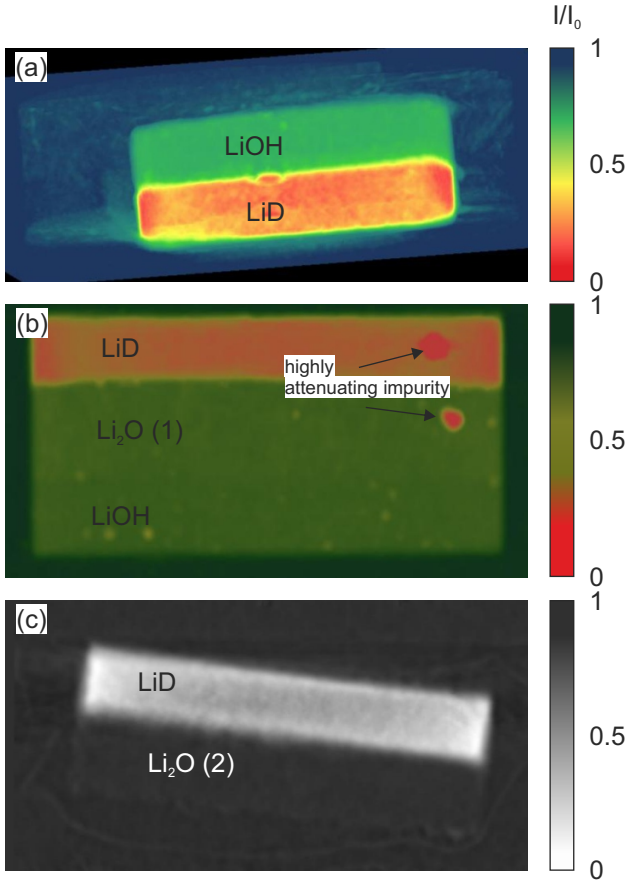

Figure 5: Three dimensional rendered volume of samples. (a) sample (4), LiD / Li$_2$O (1) (160 µm) / LiOH specimen. The intense red area is LiD and the intense green area is LiOH. The diffuse green area surrounding the sample is the sample container. (b) sample (2), LiD / Li$_2$O (1) / LiOH specimen. The intense red area is LiD and the intense green areas are Li$_2$O and LiOH. The diffuse green area surrounding the sample is the sample container. (c) sample (1) LiD / Li$_2$O (1) (50 µm) / Li$_2$O (2) sample. The bright area is LiD and the transparent area is Li$_2$O (2).

decomposition of LiOH, H_2O escapes from the material, which has been previously shown to cause cracking and spall from the surface [24]. However, there is no conclusive evidence of cracking in the Li_2O (2) layer in this sample. Small variations in neutron transmission (less than 2%) are apparent, but this is too low to assign to cracking. The fact that Li_2O (2) is highly transparent ($I/I_0 = 0.96$, table 4) hinders the observation of cracking. Indeed, the resolution of the instrument (100 µm) may not be sufficient to observe cracking, which has been previously reported to be of the order of 10 µm.

In all CT reconstructions it was clear that there was a variation in the transmitted neutron intensity of the LiD layer. This can be visualized as red/yellow/orange color variations in figures 5(a) and (b) and grayscale contrast in (c). The samples all have decreased neutron transmission at the edges and increased transmission in the core of the material. The most plausible explanation is that this effect is a result of variations in material density. Compaction of powders were performed using a uniaxial press (at a modest pressure), which is known to introduce density gradients into materials [53]. Frictional forces reduce the transmitted pressure as it progresses through a material and thus the centre of the material is less dense than the outer regions. Line profiles provide an average transmitted intensity while CT scans can provide information on a more localized scale.

4. Conclusions

Neutron radiography has been shown to be an effective technique in observing LiH and its hydrolysis products. The large differences in the relative transmission of neutrons through LiD, ^{7}LiOH and $^7Li_2O$ allow for unambiguous identification of these compounds. For these compounds, Σ was measured and compared to calculated values. Agreement was generally good, however, there was a tendency for calculation to overestimate the observed values of Σ. This deviation was ascribed to a combination of beam hardening, the fact that a polychromatic neutron source was employed, and to residual sample porosity. Neutron imaging has also proven to be effective in the observation of the thermal conversion of LiOH to Li_2O, where the loss of H in this process is clear. There is also an increase in the width of the LiD – LiOH interface, suggestive of further hydrolysis of the LiD layer. Tomographic methods give further insight into the three dimensional structure of these layers, primarily impurities, structural defects and density variations. The only detriment identified is the spatial resolution, approximately 100 µm, which precludes observing the initial stages of the hydrolysis reactions. The neutron imaging data provided here gives a basis for future research into LiH hydrolysis. In particular, the data presented here shows that three dimensional, time dependent observations of processes such as LiH hydrolysis and LiOH thermal decomposition are feasible with neutron imaging and may contribute significant additional insight into these phenomena. Furthermore, new neutron imaging facilities, such as the versatile neutron imaging instrument (VENUS) at ORNL [54] and a neutron microscope at the National Institute of Standards and Technology [55] are set to come available in the next few years. These instruments will feature intense beams and resolution on the order of 1 µm, which may open up exciting possibilities regarding imaging the early stages of LiH hydrolysis and elucidating microscopic features.

5. Acknowledgments

Funding for this research was provided by the Y-12 National Security Complex Plant Directed Research, Development and Demonstration program. The High Flux Isotope Reactor (HFIR) user facility, Oak Ridge National Laboratory, is supported by the Scientific User Facilities Division, the Office of Basic Energy Sciences, the U.S. Department of Energy. This work of authorship and those incorporated herein were in part prepared by Consolidated Nuclear Security, LLC (CNS) Pantex Plant/Y-12 National Security Complex as accounts of work sponsored by an agency of the United States Government under contract DE NA0001942. Neither the United States Government nor any agency thereof, nor CNS, nor any of their employees, makes any warranty, express or implied, or assumes any legal liability or responsibility for the accuracy, completeness, use made, or usefulness of any information, apparatus, product, or process disclosed, or represents that its use would not infringe privately owned rights. Reference herein to any specific commercial product, process, or service by trade name, trademark, manufacturer, or otherwise, does not necessarily constitute or imply its endorsement, recommendation, or favoring by the United States Government or any agency or contractor thereof, or by CNS. The views and opinions of authors expressed herein do not necessarily state or reflect those of the United States Government or any agency or contractor thereof, or by CNS. This document has been authored by CNS LLC, a contractor of the United States Government under contract DE NA0001942, or a subcontractor thereof. Accordingly, the United States Government retains a paid up, nonexclusive, irrevocable, worldwide license to publish or reproduce the published form of this contribution, prepare derivative works, distribute copies to the public, and perform publicly and display publicly, or allow others to do so, for United States Government purposes.

References

[1] C. D. Montgomerie, Nucl. Eng. Des. 25 (1973) 309. doi:10.1016/0029-5493(73)90052-6.

[2] F. H. Welch, Nucl. Eng. Des. 26 (1974) 444. doi:10.1016/0029-5493(74)90082-X.

[3] V. C. Y. Kong, D. W. Kirk, F. R. Foulkes, J. T. Hinatsu, Int. J. Hydrogen Energ. 28 (2003) 205. doi:10.1016/S0360-3199(02)00039-3.

[4] Z. Xiong, Y. S. Chua, G. Wu, W. Xu, P. Chen, W. Shaw, A. Karkamkar, J. Linehan, T. Smurthwaite, T. Autrey, Chem. Comm. 43 (2008) 5595. doi:10.1039/b812576g.

[5] P. Gislon, P. P. Prosini, Int. J. Hydrogen Energ. 36 (2011) 240. doi:10.1016/j.ijhydene.2010.09.052.

[6] D. Strawser, J. Thangavelautham, S. Dubowsky, Int. J. Hydrogen Energ. 39 (2014) 10216. doi:10.1016/j.ijhydene.2014.04.110.

[7] A. Jain, H. Miyaoka, T. Ichikawa, Int. J. Hydrogen Energ. 41 (2016) 5969. doi:10.1016/j.ijhydene.2016.02.069.

[8] P. C. Bertone, J. Nucl. Mater. 151 (1988) 281. doi:10.1016/0022-3115(88)90022-0.

[9] A. Donato, Fusion Eng. Des. 38 (1998) 369. doi:10.1016/S0920-3796(97)00123-3.

[10] H. Lu, S. T. Murphy, M. J. D. Rushton, D. C. Parfitt, D. W. Grimes, Fusion Eng. Des. 87 (2012) 1834. doi:10.1016/j.fusengdes.2012.08.008.

[11] A. Abouimrane, Y. Cui, Z. Chen, I. Belharouak, H. B. Yahia, H. Wu, R. Assary, L. A. Curtiss, K. Amine, Nano Energy 27 (2016) 196. doi:10.1016/j.nanoen.2016.06.050.

[12] W. D. Machin, F. C. Tomkins, Trans Faraday Soc. 62 (1966) 2205. doi:10.1039/tf9666202205.

[13] C. E. Holcombe, G. L. Powell, J. Nucl. Mater. 47 (1973) 121. doi:10.1016/0022-3115(73)90198-0.

[14] N. R. Smyrl, E. L. Fuller Jr, G. L. Powell, Appl. Spectrosc. 37 (1983) 38. doi:10.1366/0003702834634280.

[15] J. H. Leckey, L. E. Nulf, J. R. Kilpatrick, Langmuir 12 (1996) 6361. doi:10.1021/la950843h.

[16] C. Haertling, R. J. Hanrahan Jr, R. Smith, J. Nucl. Mater. 349 (2006) 195. doi:10.1016/j.jnucmat.2005.10.005.

[17] C. Maupoix, J. L. Houzelot, E. Sciora, G. Gaillard, S. Charton, L. Saviot, F. Bernard, Powder Technol. 208 (2011) 318. doi:10.1016/j.powtec.2010.08.023.

[18] M. B. Shauai, S. Xiao, Q. S. Li, M. F. Chu, X. F. Yang, World Acad. Sci. Eng. Tech. 5 (2011) 979.

[19] S. Xiao, M. B. Shauai, M. F. Chu, World Acad. Sci. Eng. Tech. 5 (2011) 2203.

[20] R. Ren, A. L. Ortiz, T. Markmaitree, W. Osborn, L. L. Shaw, J. Phys. Chem. B 110 (2006) 10567. doi:10.1021/jp060068m.

[21] R. P. Awbery, D. A. Broughton, S. C. Tsang, J. Nucl. Mater. 373 (2008) 94. doi:10.1016/j.jnucmat.2007.05.039.

[22] L. N. Dinh, C. M. Cecala, J. H. Leckey, M. Balooch, J. Nucl. Mater. 295 (2001) 193. doi:10.1016/S0033-3115(01)00548-7.

[23] L. N. Dinh, W. Mclean II, M. A. Schildback, J. D. LeMay, W. J. Siekhaus, M. Balooch, J. Nucl. Mater. 317 (2003) 175. doi:10.1016/S0022-3115(03)00084-9.

[24] L. N. Dinh, D. M. Grant, M. A. Schildback, R. A. Smith, W. J. Siekhaus, B. Balazs, J. H. Leckey, J. R. Kirkpatrick, W. Mclean II, J. Nucl. Mater. 347 (2005) 31. doi:10.1016/j.nucmat.2005.06.025.

[25] J. Phillips, M. C. Bradford, M. Klanchar, Energy Fuels 9 (1995) 569. doi:10.1021/ef00052a001.

[26] J. Guichard, F. Bouyer, E. Sciora, F. Bernard, H. Lecoq, R. Besnard, J. P. Bellat, Int. J. Hydrogen Energ. 40 (2015) 12736. doi:10.1016/j.ijhydene.2015.07.047.

[27] S. M. Myers, J. Appl. Phys. 45 (1974) 4320. doi:10.1063/1.1663052.

[28] G. L. Powell, M. Milosevic, J. Lucania, N. J. Harrick, Appl. Spectrosc. 46 (1992) 111. doi:10.1366/0003702924444272.

[29] A. Anderson, F. Lüty, Phys. Rev. B 28 (1983) 3415. doi:10.1103/PhysRevB.28.3415.

[30] A. C. Stowe, N. Smyrl, Vibrat. Spec. 60 (2012) 133. doi:10.1016/j.vibspec.2012.01.018.

[31] A. Sifuentes, A. C. Stowe, N. Smyrl, J. Alloy. Compd. 580 (2013) S271. doi:10.1016/j.jallcom.2013.02.046.

[32] R. S. Calder, W. Cochran, D. Griffiths, R. D. Lowde, J. Phys. Chem. Solids 23 (1962) 621. doi:10.1016/0022-3697(62)90522-X.

[33] M. Krzystyniak, S. E. Richards, A. G. Seel, F. Fernandez-Alonso, Phys. Rev. B 88 (2013) 184304. doi:10.1103/PhysRevB.88.184304.

[34] W. Wang, Q. Li, Q. Li, X. Yang, G. Le, Mater. Sci. Tech. 32 (2016) 434. doi:10.1179/1743284715Y.0000000105.

[35] Y. Ishii, Y. Morii, R. M. Nicklow, S. Funahashi, Physica B 213-214 (1995) 436. doi:10.1016/0921-4526(95)00362-D.

[36] K. Herbrig, C. Pohlmann, L. Gondek, H. Figiel, N. Kardjilov, A. Hilger, I. Manke, J. Banhart, B. Kieback, L. Röntzsch, J. Power Sources 293 (2015) 109. doi:10.1016/j.jpowsour.2015.05.039.

[37] E. Staritzky, D. I. Walker, Anal. Chem. 28 (1956) 1055. doi:10.1021/ac60114a043.

[38] L. Crow, L. Robertson, H. Bilheux, M. Fleenor, E. Iverson, X. Tong, D. Stoica, W. T. Lee, Nucl. Instrum. Methods Phys. Res. A 643 (2011) S71. doi:10.1016/j.nima.2010.06.213.

[39] E. H. Lehmann, P. Vontobel, N. Kardjilov, Appl. Rad. Isot. 61 (2004) 503. doi:10.1016/j.apradiso.2004.03.075.

[40] E. H. Lehmann, N. Kardjilov, in: J. Banhart (Ed.), Advanced Tomographic Methods in Materials Research and Engineering, Oxford University Press, 2008, pp. 376–408.

[41] E. H. Lehmann, A. Kaestner, L. Josic, S. Hartmann, D. Mannes, Nucl. Instrum. Methods Phys. Res. A 651 (2011) 161. doi:10.1016/j.nima.2010.11.191.

[42] P. Zhang, F. H. Wittmann, T. J. Zhao, E. H. Lehmann, P. Vontobel, Nucl. Eng. Des. 241 (2011) 4758. doi:10.1016/j.nucengdes.2011.02.031.

[43] A. Carminati, A. Kaestner, R. Hassanein, O. Ippisch, P. Vontobel, H. Flühler, Adv. Water Res. 30 (2007) 1168. doi:10.1016/j.advwatres.2006.10.006.

[44] R. Satija, D. L. Jacobson, M. Arif, S. A. Werner, J. Power Sources 129 (2004) 238. doi:10.1016/j.jpowsour.2003.11.068.

[45] K. Ryzewski, S. Herringer, H. Bilheux, L. Walker, B. Sheldon, S. Voisin, J. C. Bilheux, V. Finocchiaro, Physics Procedia 43 (2013) 343. doi:10.1016/j.phpro.2013.03.041.

[46] S. F. Mughabghab, M. Divadeenam, N. E. Holden, Neutron Cross Sections, volume 1, Academic Press, New York, NY, USA, 1981.

[47] V. F. Sears, Neutron News 3 (1992) 26. doi:10.1080/10448639208218770.

[48] W. M. Stacey, Nuclear Reactor Physics, 2nd ed., Wiley, Weinheim, Germany, 2007.

[49] N. E. Holden, in: W. Haynes (Ed.), Handbook of Chemistry and Physics, 93rd edition, CRC Press, 2012, pp. 11–175.

[50] F. Kharfi, M. Bastuerk, A. Boucenna, Nucl. Instrum. Methods Phys. Res. A 565 (2006) 416. doi:10.1016/j.nima.2006.06.042.

[51] N. Hachouf, F. Kharfi, A. Boucenna, Appl. Rad. Isot. 70 (2012) 2355. doi:10.1016/j.apradiso.2012.06.017.

[52] N. Hachouf, F. Kharfi, M. Hachouf, A. Boucenna, Appl. Rad. Isot. 107 (2016) 353. doi:10.1016/j.apradiso.2015.11.024.

[53] S. Stupkiewicz, A. Piccolroaz, D. Bigoni, J. Euro. Ceram. Soc. 34 (2014) 2839. doi:10.1016/j.jeurceramsoc.2013.11.017.

[54] H. Bilheux, K. Herwig, S. Keener, L. Davis, Physics Procedia 69 (2015) 55. doi:10.1016/j.phpro.2015.07.007.

[55] D. Liu, D. Hussey, M. V. Gubarev, B. D. Ramsey, D. Jacobson, M. Arif, D. E. Moncton, B. Khaykovich, Appl. Phys. Lett. 102 (2013) 183508. doi:10.1063/1.4804178.